Hindawi
Advances in Materials Science and Engineering
Volume 2022, Article ID 5260159, 14 pages
https://doi.org/10.1155/2022/5260159

*Research Article*

# Investigating the Effect of Calcium Lignosulfonate on the Durability and Performance of Asphalt Mixtures

**Saeed Fatemi, Jafar Bolouri Bazaz, and Seyed Ali Ziaee**

*Department of Civil Engineering Engineering Faculty, Ferdowsi University of Mashhad, Mashhad, Iran*

Correspondence should be addressed to Seyed Ali Ziaee; sa-ziaee@um.ac.ir

Received 8 September 2021; Revised 18 February 2022; Accepted 2 March 2022; Published 31 March 2022

Academic Editor: Ramadhansyah Putra Jaya



Using bitumen modifiers to prolong the asphalt mixture's life has been considered a practical approach in constructing asphalt mixtures. Among various bitumen modifiers, biomass ones have been more noteworthy because of their abundance, cost-effectiveness, renewability, and sustainability. Calcium lignosulfonate (CLS), as a plant-based bitumen modifier, has been studied to enhance the rheological properties of bitumen. However, the feasibility of using CLS as a rutting retarder of asphalt mixtures is still unclear. This study focused on the durability of asphalt mixtures containing CLS powder as a bitumen modifier. Specifically, extensive laboratory tests were conducted to determine the performance of asphalt mixtures against traffic loadings. In this study, to begin, CLS-modified bitumen was manufactured using a high-shear mixer at various CLS dosages (5, 10, 15, and 20 wt.%). Afterward, the optimum bitumen content of asphalt mixtures was found using the Marshall mix design technique. Finally, a series of dynamic tests, including resilient modulus, dynamic creep, and wheel-tracking tests, were combined with Zhou's three-stage model and Tukey method to determine the influence of CLS on asphalt mixture's rutting potential. The Tukey method found that asphalt mixtures containing 15% CLS had the highest rutting performance among the samples tested under repetitive loadings. Meanwhile, the surface morphology and elemental analysis of CLS powder were investigated using a field emission scanning electron microscope (FESEM) and by energy-dispersive X-ray spectroscopy (EDX), respectively. The FESEM and EDX results showed that the CLS powder had a bumpy structure and its chemical structure contained metal oxide, carbon, magnesium, calcium, and silicon. The results indicated that the asphalt mixtures became stiff owing to the combination of CLS and bitumen, which significantly affected the rutting improvement of asphalt mixtures. Moreover, Zhou's three-stage model revealed that the incorporation of CLS into bitumen enhanced the rutting resistance capacity of asphalt mixtures against traffic loadings.

## 1. Introduction

Nowadays, asphalt mixtures are used as a significant material for road construction because of their good performance, comfort, and ease of maintenance [1, 2]. Asphalt mixtures consist of two major constituents, namely, stone skeleton and bitumen [3]. The pavements surface layer, constructed by the asphalt mixture, transfers compressive stress from the top to the bottom layer [4]. Moreover, the surface layer protects the pavement's body against environmental factors, including moisture damage, UV radiation, and oxygen [5]. When traffic loadings are conducted on asphalt mixtures, the serviceability of roads encounters degradation due to premature distress, including rutting, cracking, and fatigue failure [6, 7]. They can reduce the service life of pavements; therefore, the need for rehabilitation, which requires spending money and time, increases [8].

Rutting can be defined as the progressive accumulation of small deformations that occur by densification and shear deformations under applied traffic loadings [9]. Among the asphalt mixture's premature distress, rutting is more noticeable because it increases the risk of human life by disturbing pavements smooth and safe surface for vehicles to commute [10]. Therefore, rutting leads to endangering road safety and increases the burden on governments by increasing road maintenance costs [11, 12].

Various research studies have been conducted to determine how well asphalt mixtures resist rutting. Researchers showed that although bitumen formed a small

proportion of the total weight of asphalt mixtures, bitumen significantly affected the rutting potential of asphalt mixtures [13, 14]. Then, various bitumen modifiers have been studied to enhance the positive effects of bitumen on the rutting performance of asphalt mixtures. De Melo et al. [15] used carbon nanotubes for bitumen modification. The results revealed that carbon nanotubes increased the asphalt mixture's performance; moreover, they improved the rutting resistance of asphalt mixtures. Yoo et al. [16] conducted an experimental work on the combination of polypropylene and bitumen; their findings showed that polypropylene could enhance the rutting resistance of asphalt mixtures. In 2020, Ghanoon et al. [17] conducted experimental research and used styrene–butadiene–styrene (SBS) as a bitumen modifier. The findings indicated that the SBS-modified bitumen had a positive effect on the rutting behavior of asphalt mixtures.

Biomass materials have been more noteworthy for researchers among bitumen modifiers because of their abundance, cost-effectiveness, renewability, and sustainability [18]. Lignin, obtained from the biofuel and paper industries, is classified as a significant waste biomass material [19]. Lignin has the adequate capability to be used as a bitumen modifier because lignin's chemical structure contains reactive chemical compounds that can be employed to modify petroleum chemical substances [20]. Moreover, the chemical structure of lignin is comparable to petroleum bitumen's chemical structure [21]. Several investigations have examined the utilization of lignin as a bitumen modifier or extender. Batista et al. [22] studied the effect of lignin, sourced from the pulp industry, on the aging performance of bitumen. The results revealed that lignin could retard bitumen's aging process.

Similarly, Xu et al. [23] indicated that although lignin in bitumen could enhance bitumen's aging resistance, incorporating lignin into bitumen degraded the fatigue performance of modified bitumen. In 2020, apart from the role of lignin in bitumen modification, Zhang et al. [24] examined the influence of lignin fibers on the mechanical characteristics of asphalt mixtures. The results exhibited the positive effect of lignin fibers on the asphalt mixture's mechanical properties, including abrasion resistance, fatigue life, and moisture damage.

The rutting potential of asphalt mixtures can be assessed by two main laboratory methods: (1) static tests and (2) dynamic tests [25]. The former consists of static creep, indirect tensile, and Marshall tests; the latter contains dynamic creep, wheel tracking, and resilient modulus tests [26]. Researchers believe that dynamic tests are more accurate than static tests to appraise the asphalt mixture's rutting susceptibility [27]. Among dynamic tests, the dynamic creep test is considered one of the most effective techniques because laboratory outputs achieved by the dynamic creep test have a reasonable correlation with accumulated strains that occurred under repetitive loading on-field situations [28]. It is worth mentioning that the wheel-tracking test can determine the exact rut depth of asphalt mixtures [29].

Comprehensive research has been carried out regarding creation models to assess and predict the creep potential of asphalt mixtures. The outputs of the dynamic creep test have been proposed for application in creep models because the creep curve depicts the asphalt mixture's rutting performance based on the accumulation of permanent strain versus the load repetition [30]. Previous research studies revealed that creep models, including those by Barksdale, Monismith, Ohio State, and Superpave, could not precisely describe the creep curve of asphalt mixtures [31]. In 2004, Zhou [31] defined three stages for describing the rutting creep curve; moreover, he located two transition points between stages [32].

Different types of lignin can be categorized based on their chemical structure [33]. Organosolv lignin is obtained from wood processing using liquid organic solvents to treat wood chips [34]. Kraft lignin emanates from the pulping process, converting coniferous wood to pulp [35]. Klason lignin comes from the acid hydrolysis process of wood [36]. Applying the enzymatic hydrolysis method to produce bio-ethanol leads to the formation of enzymatic hydrolysis lignin [37]. Sulfonated lignin emanates from black liquor; moreover, sulfonated lignin is a nontoxic polymer [38]. Calcium lignosulfonate (CLS) emanates from the sulfite pulping process, leading to manufacturing of paper from softwood; moreover, CLS is a brownish powder and an amorphous polymer [39].

The annual production of CLS is estimated to be 50 million tons, but only one-half of them can be utilized. Therefore, the use of CLS for the construction of asphalt mixtures can reduce the consumption of natural materials and reduce the mass of CLS that ends up in landfills [40]. This study aims to investigate the rutting performance of asphalt mixtures containing CLS-modified bitumen because CLS contains chemical groups that tend to dissolve in petroleum-based materials; therefore, its solubility potential in bitumen is more than in lignin [41]. Moreover, the rutting performance of asphalt mixtures containing CLS-modified bitumen has barely been investigated.

## 2. Materials and Methods

*2.1. Aggregate.* In this experimental research, the stone skeleton of the asphalt mixture consists of two principal objects—crushed aggregates and mineral filler—supplied from the limestone quarry. It has been used as the primary source for constructing asphalt mixtures in Mashhad, Iran's northeastern province [42]. X-ray fluorescence (XRF) analysis was used to assess the chemical composition of aggregates. An ARL PERFORM'X spectrometer was used to conduct the above-mentioned analysis [43]. The weight proportions of the major oxides are shown in Table 1 using the bulk chemical analysis approach. Moreover, the physical properties of the aggregates were obtained for comparison with the specification limits (Table 2).

Based on the No. 4 gradation of the Iran Road Pavement Code, an upper and a lower limit were given for the construction of asphalt mixtures (Figure 1) [44]. As seen in Figure 1, the selected gradation was within the top and lower bounds. It is worth mentioning that the selected gradation is the preferred aggregate gradation for the construction of asphalt mixtures among consultants and contractors in Iran [42].

Table 1: Chemical composition of aggregates.

| Constituent | MgO | $Al_2O_3$ | $SiO_2$ | $K_2O$ | CaO | $Fe_eO_3$ | Loi (950°C) |
|---|---|---|---|---|---|---|---|
| Wt. (%) | 17.6 | 0.03 | 0.29 | 0.06 | 35 | 0.22 | 46.8 |

Table 2: Physical characteristics of the coarse and fine aggregates.

| Test properties<br>Coarse aggregate | Unit | Value | Standard ASTM | Specification limit |
|---|---|---|---|---|
| Los Angeles abrasion value | % | 21 | C131 | ≤25 |
| Fractured particles in one side | % | 96 | D5821 | ≥95 |
| Fractured particles in two sides | % | 92 | D5821 | ≥90 |
| Bulk specific gravity | Gr/ $m^3$ | 2.66 | C127 | – |
| Apparent specific gravity | Gr/ $m^3$ | 2.74 | C127 | – |
| Water absorption | % | 0.84 | C127 | ≤2.5 |
| Fine aggregate | | | | |
| Bulk specific gravity | Gr/ $m^3$ | 2.66 | C128 | – |
| Apparent specific gravity | Gr/ $m^3$ | 2.87 | C128 | – |
| Water absorption | % | 3.3 | C128 | ≤2.5 |
| Sand equivalent | % | 74 | D2419 | ≥50 |

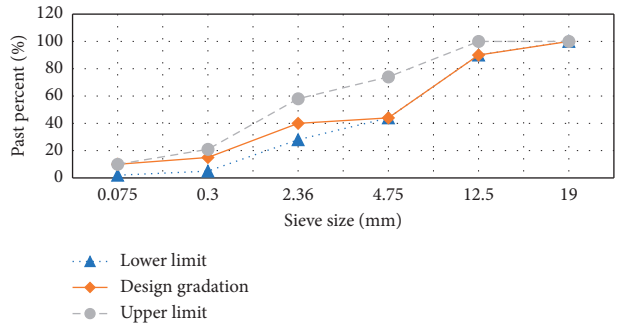


Figure 1: Upper, lower, and selected criteria for aggregate gradation.

*2.2. Bitumen.* This research employed the 60/70 penetration grade-paving bitumen supplied from the Shargh Oil Refinery (Mashhad, Iran). Table 3 shows its physical properties. The mentioned bitumen is compatible with Iran's climate conditions [45].

*2.3. Calcium Lignosulfonate.* Calcium lignosulfonate (CLS) is a recovered powder made from lignin, a residue of the wood and paper industries [46]. CLS provided for this study was light yellow–brown in color; in addition, its CAS number was 8061-52-7, and Ligno Tech South Africa Co. Ltd. provided this powder. In Table 4, there is some information about the essential characteristics of CLS. A field emission scanning electron microscope (FESEM) was employed to determine CLS powder's surface morphology [47]. According to Figure 2, the CLS surface had a bumpy structure. Simultaneously, the energy-dispersive X-ray spectroscopy (EDX) analysis was carried out to determine the elemental composition of CLS powder [48]. According to Table 5, the major constituents of CLS powder were metal oxide, carbon, magnesium, calcium, and silicon.

*2.4. CLS-Modified Bitumen.* At 160°C, a high-shear mixer with a rotational speed of 3000 rpm was employed for 30 minutes to incorporate CLS powder into virgin bitumen [49]. Jedrzejczal and others [50] showed that the maximum amount of lignin powder mixed into bitumen could not exceed 20% because of the economic factors of the road construction process. Therefore, the incorporation of CLS into bitumen was limited to 20% during this study. In this experimental research, four percentages of CLS powder (5%, 10%, 15%, and 20%) were blended with virgin bitumen (by weight of bitumen). The key advantage of incorporating four levels of CLS into bitumen was to evaluate the effectiveness of CLS on the durability and performance of asphalt mixtures based on the comparative approach.

## 3. Research Approach

According to ASTM D1559, the control samples optimum bitumen content (OBC) was first determined using the Marshall mix design technique. For the determination of OBC, three Marshall samples of each bitumen content (4%, 4.5%, 5%, 5.5%, 6%, and 6.5%) were fabricated by 75 blows of the Marshall hammer on each side of the asphalt mixtures. The OBC of the control sample was then determined based on Marshall design parameters, including stability, flow, air void content, bulk density, and voids in mineral aggregates (VMA). After determining the OBC of the control sample, it was considered for fabricating the CLS-modified Marshall samples. At the next step, cylindrical samples were

Table 3: The virgin bitumen's physical characteristics.

| Test properties | Standard ASTM | Unit | Test result |
|---|---|---|---|
| Penetration @ 25 °C | D5 | 0.1 mm | 67 |
| Softening point | C36 | °C | 51 |
| Viscosity @ 135 °C | | Pa.s | 0.354 |
| Specific gravity | D70 | Gr/ $cm^3$ | 1.02 |
| Ductility @ 25 °C | D113 | Cm | +100 |
| Flash point | D92 | °C | 280 |
| PG | | - | 64–16 |

Table 4: Physical properties of the CLS powder.

| Test | Unit | Results |
|---|---|---|
| Color | — | Light brown |
| Dry matter | % min | 93.0 |
| PH (10% solution) | — | $7.5 \pm 0.8$ |
| Insolubility (v/v) | % Max | 0.5 |
| Bulk density | kg/ $m^3$ | 500 |
| Reducing sugars | % | 3 |

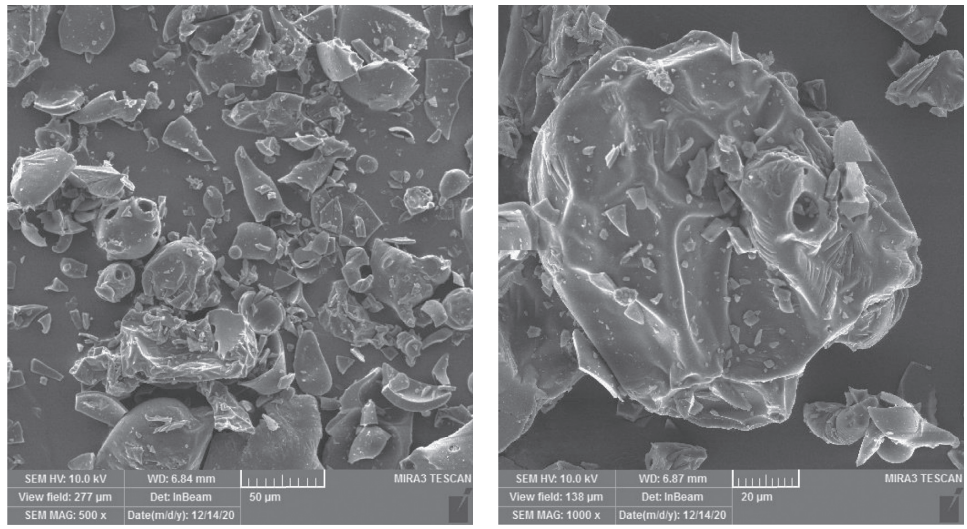


(a) (b)

Figure 2: The FESEM images of CLS powder taken at (a) 500x zoom and (b) 1000x zoom.

Table 5: Elemental analysis of CLS powder by EDX.

| Elt | Line | Int | Error | K | Kr | W% | A% | Zaf | Ox% | Pk/Bg |
|---|---|---|---|---|---|---|---|---|---|---|
| C | Ka | 20.0 | 4.4546 | 0.2282 | 0.0929 | 23.70 | 31.61 | 0.3920 | 0.00 | 75.92 |
| O | Ka | 82.9 | 4.6018 | 0.4700 | 0.1914 | 59.57 | 59.65 | 0.3212 | 0.00 | 954.11 |
| Mg | Ka | 50.9 | 1.5427 | 0.1030 | 0.0419 | 7.26 | 4.78 | 0.5777 | 0.00 | 30.88 |
| Al | Ka | 2.3 | 1.5659 | 0.0045 | 0.0018 | 0.30 | 0.18 | 0.6229 | 0.00 | 3.36 |
| Si | Ka | 6.3 | 1.5891 | 0.0131 | 0.0053 | 0.73 | 0.41 | 0.7346 | 0.00 | 5.37 |
| Ca | Ka | 45.2 | 0.5246 | 0.1812 | 0.0738 | 8.45 | 3.38 | 0.8738 | 0.00 | 31.25 |
| | | | | 1.0000 | 0.4073 | 100.00 | 100.00 | | 0.00 | |

manufactured using a Superpave gyratory compactor (SGC) for resilient modulus and dynamic creep tests. Moreover, during the wheel-tracking test, a kneading compactor was employed to prepare slab specimens for rut depth calculation.

*3.1. Marshall Stability Parameters.* The determination of Marshall parameters for asphalt mixtures involved several steps. The Marshall hammer was used to first manufacture a total of 15 Marshall samples. Second, the manufactured samples were classified into five categories based on their CLS

content. It is worth mentioning that the compaction energy for sample preparation was equally simulated to heavy traffic loadings (i.e., 75 blows on each side of the asphalt mixtures) by the Marshall hammer [51]. After the compaction process, the Marshall stability, flow value, and Marshall quotient (MQ) were determined according to ASTM D1559 [52].

Marshall stability depends on the pressure loading applied on samples during the Marshall test. Therefore, Marshall stability can be defined as a specimens maximum bearing capacity under uniform vertical loading [53]. The samples deformation during vertical loading up to the maximum load denotes the flow value [54]. The Marshall quotient is calculated by dividing the Marshall stability by the flow value [55]. Higher MQ values indicate higher stiffness and better resistance against traffic loadings [56].

*3.2. Resilient Modulus.* The elastic stiffness of samples was determined by the resilient modulus test. The correlation between the applied load and the sample's deformation during repetitive loadings denotes the stiffness value [57]. Compared to the asphalt mixture's strength, the resilient modulus test is nondestructive because the load suffered by the sample is negligible [58].

The resilient modulus can calculate the optimum pavement thickness to design a new pavement [42]. In this research, the resilient modulus test was conducted at a temperature of 25°C with a haversine loading applied on samples using a universal testing machine (UTM) according to ASTM D4123 [59]. Figure 3 shows the resilient modulus test's loading pattern and testing machine. After 15 cycles of preloading, the computer software determined the average values at the last five cycles. Afterward, the resilient modulus was determined using the following equation [42]:

$$M_r = \frac{P(\nu + 0.27)}{t\Delta H}, \tag{1}$$

where $M_r$ is the resilient modulus, P is the repetitive load (N), $\nu$ is Poisson's coefficient, $\Delta H$ is the average of reversible horizontal deformations (mm), and $t$ is the specimen thickness (mm) [60]. It is worth mentioning that Poisson's coefficient was equal to 0.35 based on the test temperature [42]. Table 6 presents the setup parameters of the resilient modulus test.

*3.3. Dynamic Creep Test.* The dynamic creep test determines the tendency of asphalt mixtures to permanent deformations [61]. Cyclic loadings are applied to the specimens during the dynamic creep test to simulate actual traffic loads [62]. The significant outcome of the dynamic creep test is the vertical deformation against the loading cycles. While the dynamic creep test outputs do not correspond to the real rut depth, they can compare the rutting resistance of various asphalt mixtures [32].

As depicted in Figure 4, the creep curve obtained from the dynamic creep test can be divided into three zones. The creep strain rate increases sharply in the first phase due to the compaction process of the asphalt mixture [30]. The second phase involves an approximately constant strain rate. The creep strain rate experiences an upward trend at the beginning of the tertiary phase, which denotes rutting failure [42]. The flow number (FN) can then be defined as the number of loading cycles at the beginning of the tertiary phase. Researchers determine the FN value as a benchmark to compare the rutting potential of asphalt mixtures [42, 63].

This study conducted the dynamic creep test on specimens of asphalt mixtures by UTM-14 at the Ferdowsi University of Mashhad following the AS-2891.12.1 standard (Figure 4) [64]. At the beginning of the dynamic creep test, samples were subjected to a static preloading stress of 10 kPa, which took 5 minutes to establish proper contact between the sample's surface and the loading's platen [42]. After the preloading stage, a cyclic stress level of 400 kPa with a frequency of 5 Hz was applied to the samples. The dynamic creep test was conducted at 50°C. Moreover, samples were treated at a temperature of 50°C for four hours before starting the test due to providing homogenous temperature within asphalt mixtures. Table 7 summarizes the required variables of the dynamic creep test.

*3.4. Wheel Tracking Test.* The Hamburg wheel-tracking (HWT) test has been used to measure the rut depth caused by the rolling wheel (Figure 5) [65]. The HWT outputs show the permanent deformations emanating from applying cyclic loadings on the surface of asphalt mixtures [57]. The HWT test was performed on 300 × 300 × 50 mm compacted slabs with a 4% air void content at 50°C following the AASHTO T324 code (Figure 5) [66]. Moreover, the rubber wheel with an average contact stress of 50 psi was subjected to the slab samples with a 52 + 2 passes/minute loading rate [67]. A linear variable differential transformer (LVDT), placed at the side of the wheel, measured the rut depth data at each cycle. The HWT test was automatically terminated after 120 minutes. Figure 5 illustrates the HWT test apparatus and the compacted slab of the asphalt mixture.

The value of the wheel-tracking slope in the air ($WTS_{air}$), which denotes the grade of the deformation on the track for 1000 load cycles, was calculated using the following equation [68]:

$$WTS_{air} = \frac{(d_{6000} - d_{3000})}{3}, \tag{2}$$

where $WTS_{air}$ corresponds to the wheel-tracking slope (mm/$10^3$ load cycles) and $d_{3000}$ and $d_{6000}$ denote the rut depth values (mm) at 3000 and 6000 load cycles, respectively.

It is worth mentioning that the RD value, which indicates the total rut depth at the termination time (120 minutes), was determined [69]. To analyze the dynamic stability of asphalt mixtures, the DS parameter was obtained by the following equation [70]:

$$DS = \frac{N(t_2 - t_1)}{d_2 - d_1}, \tag{3}$$

where DS corresponds to the dynamic stability (cycle/min); $d_1$ and $d_2$ are the deformations of the asphalt mixture at rutting times $t_1$ and $t_2$, respectively (min); and N corresponds to the rolling rate (52 cycles/min).

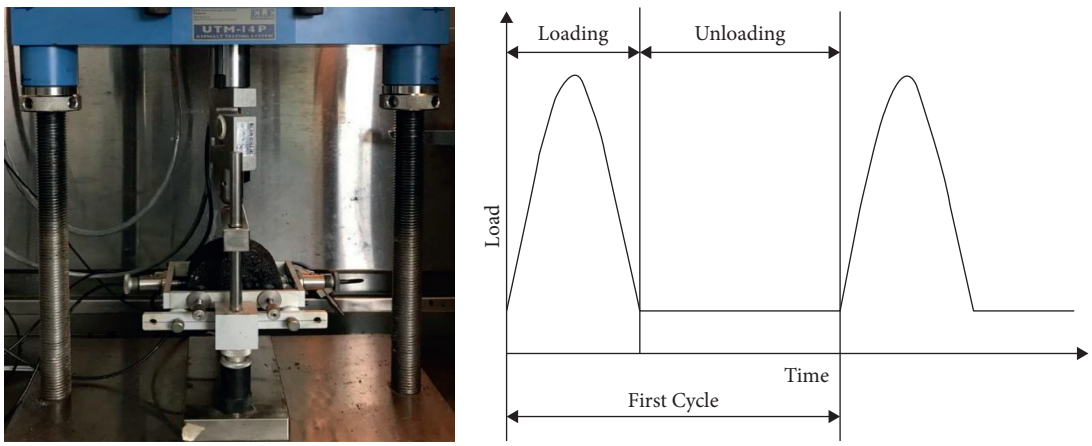


Figure 3: Resilient modulus test: (a) resilient modulus test apparatus and (b) loading shape.

Table 6: Setup parameters of the resilient modulus test.

| Parameter | Unit | Value |
|---|---|---|
| Temperature | °C | 25 |
| Applied load | N | 650 |
| Poisson's ratio | — | 0.35 |
| Loading period | ms | 100 |
| Rest period | ms | 900 |

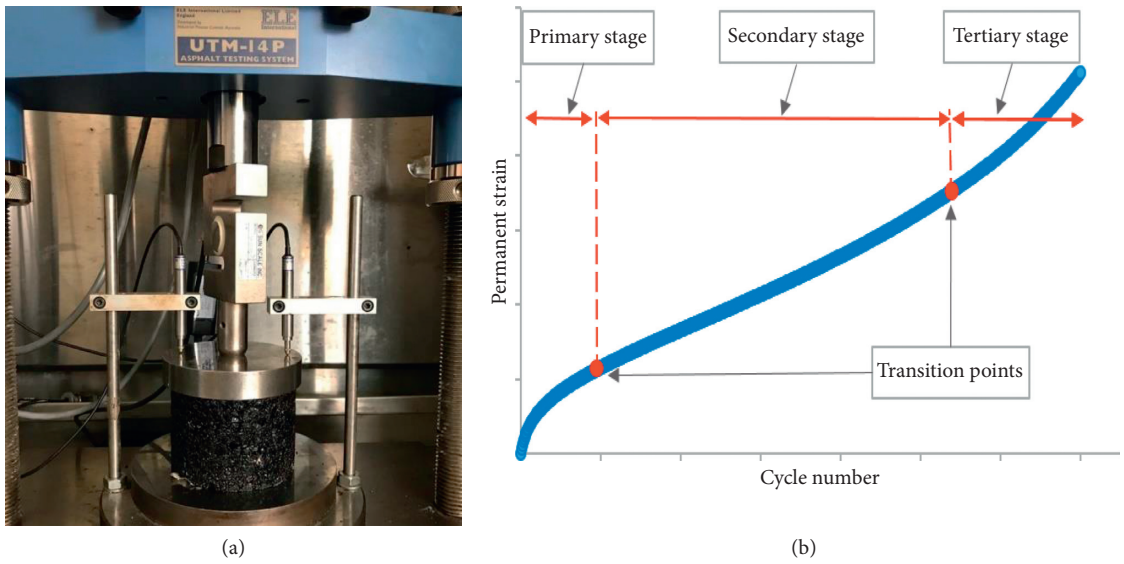


Figure 4: Dynamic creep test: (a) dynamic creep test apparatus and (b) permanent strain curve.

Table 7: Variables of the dynamic creep test.

| Parameter | Unit | Value |
|---|---|---|
| Loading pattern | — | Rectangular |
| Rest period | ms | 750 |
| Loading period | ms | 250 |
| Contact stress | kPa | 10 |
| Applied repeated stress | kPa | 400 |
| Termination criteria | — | Until the tertiary stage appeared |

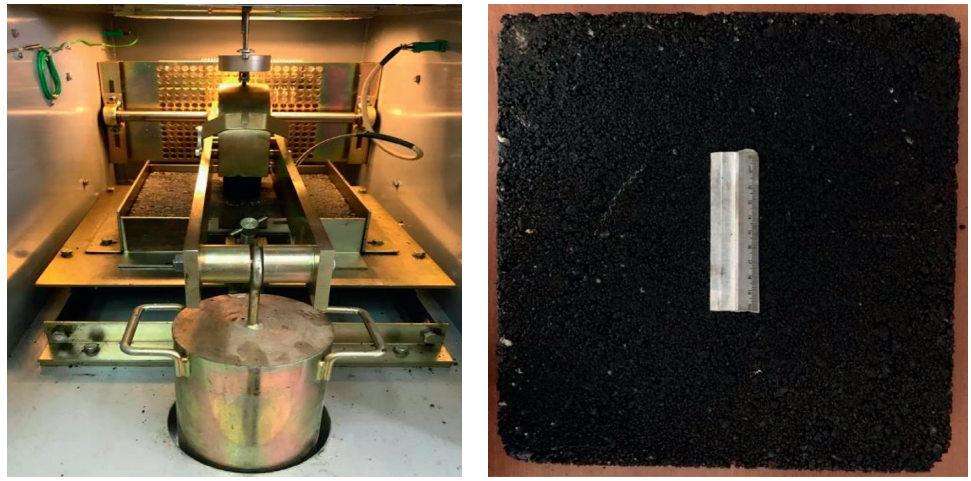

(a) (b)

Figure 5: Wheel-tracking test: (a) wheel-tracking test apparatus and (b) manufactured slab of asphalt mixture.

*3.5. Outline of Zhou Model and Tukey Method.* Zhou considered three separate stages for creep behavior of asphalt mixtures based on the permanent deformation curve [27]. The power–law function was recommended to define the primary stage. The second stage was then described using a linear function. Finally, the exponential function was proposed to predict the tertiary stage [31]. The three-stage permanent deformation model proposed by Zhou can be calculated based on the following equations [27]:

$$N \le N_{\mathrm{PS}}, \quad \varepsilon_P = \mathrm{aN}^b, \tag{4a}$$

$$\begin{aligned} &N_{\mathrm{PS}} \le N \le N_{ST}, \\ &\varepsilon_{\mathrm{PS}} = \mathrm{aN}_{\mathrm{PS}}^b, \\ &\varepsilon_P = \varepsilon_{\mathrm{PS}} + C\left(N - N_{\mathrm{PS}}\right), \end{aligned} \tag{4b}$$

$$\begin{aligned} &N \ge N_{\mathrm{ST}}, \\ &\varepsilon_{\mathrm{ST}} = \varepsilon_{\mathrm{PS}} + C\left(N_{\mathrm{ST}} - N_{\mathrm{PS}}\right), \\ &\varepsilon_P = \varepsilon_{\mathrm{ST}} + d\left(e^{f\left(N - N_{\mathrm{ST}}\right)} - 1\right), \end{aligned} \tag{4c}$$

where a, $b$, c, $d$, e, and $f$ are the material constants; $N_{\mathrm{PS}}$ and $N_{\mathrm{ST}}$ denote to the number of load repetitions corresponding to the end of the primary and secondary stages, respectively; furthermore, $\varepsilon_{\mathrm{PS}}$ and $\varepsilon_{\mathrm{ST}}$ correspond to the permanent strain at the end of the primary and secondary stages, respectively.

This study calculated the permanent strain per cycle using UTM software for each sample during the dynamic creep test. In the next step, $N_{\mathrm{PS}}$, $N_{\mathrm{ST}}$, $\varepsilon_{\mathrm{PS}}$, and $\varepsilon_{\mathrm{ST}}$ were determined according to Zhou's three-stage permanent deformation model. In addition, the one-way analysis of variance (ANOVA) was used to determine the effect of CLS on the creep behavior of the asphalt mixtures. The Tukey method with a 95% confidence level was also considered to rank the creep performance of asphalt mixtures [71].

## 4. Results and Discussion

In order to calculate the optimum bitumen content (OBC) of control asphalt mixtures, their Marshall design parameters are summarized in Table 8. According to the Iran Road Pavement Code, the OBC of control asphalt mixtures was the average of values achieved based on the following criteria:

(1) The OBC should provide 4% air voids within the compacted asphalt mixture.
(2) The OBC presents the maximum stability of the compacted asphalt mixture.
(3) The OBC brings the maximum specific gravity for compacted asphalt mixture.

After the determination of OBC, other Marshall design parameters, including voids in mineral aggregates (VMA), voids filled with bitumen (VFB), and flow values, were checked whether they satisfied the local code specification limits. The determined OBC for the control asphalt mixture was 4.9%. It is worth mentioning that the OBC of the control sample was selected to prepare CLS-modified samples.

*4.1. Marshall Stability Parameters.* When the OBC of the asphalt mixture was obtained, the Marshall stability parameters were determined for the five combinations categorized based on the CLS content. Figure 6(a) shows that the Marshall stability values experienced an upward trend versus an increment in the CLS content from 0% to 15%. Additional CLS within the bitumen from 15% to 20% decreased the Marshall stability value from 7.26 kN to 6.67 kN, respectively. Furthermore, the asphalt mixture containing 15% CLS shows a 31% increase in the Marshall stability value compared with the control asphalt mixtures. Figure 6(b) shows that the CLS-modified samples recorded lower flow values than the control sample; moreover, the asphalt sample

Table 8: Fitted equations of the Marshall design parameters.

| Marshall parameter | Unit | Fitted equation | R-squared |
|---|---|---|---|
| Marshall stability | kN | $y = -5750x^2 + 542.04x - 7.38$ | 0.956 |
| Flow | mm | $y = -1328.6x^2 + 182.87x - 2.08$ | 0.954 |
| Unit weight | gr/m$^3$ | $y = -292.86x^2 + 31.44x + 1.59$ | 0.977 |
| Air voids | % | $y = 4821.4x^2 - 726.82x + 28.34$ | 0.968 |
| VMA | % | $y = 10257x^2 - 1024.8x + 39.86$ | 0.983 |
| VFB | % | $y = -19071x^2 + 3510.5x - 55.95$ | 0.961 |

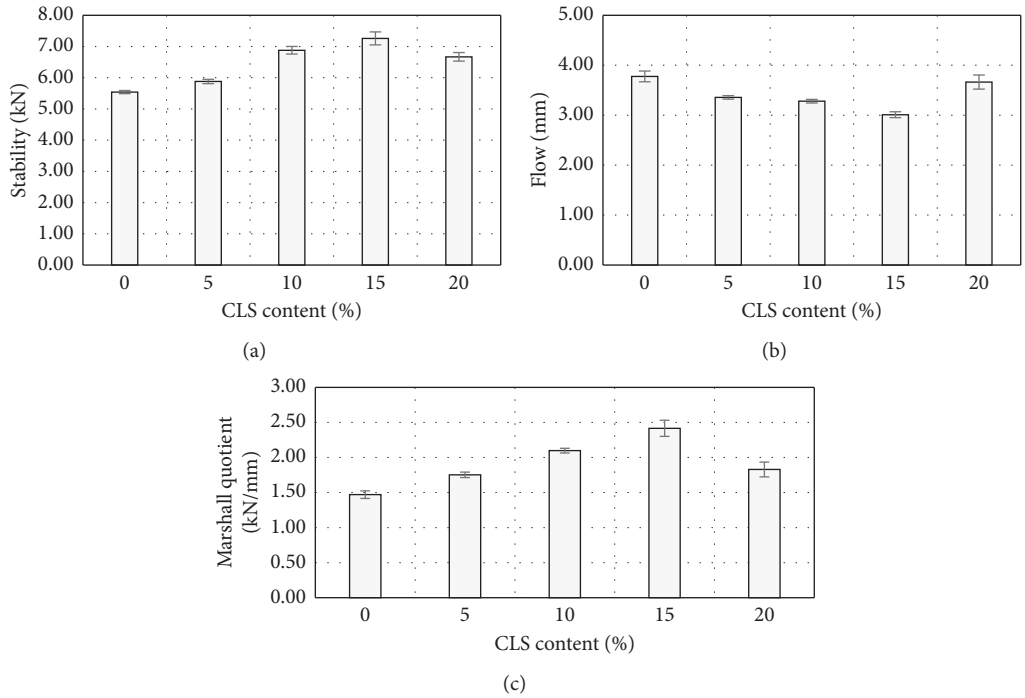


Figure 6: Marshall tests results: (a) Marshall stability outputs, (b) Marshall flow values, and (c) Marshall quotient results.

containing 15% CLS had the lowest flow value among all samples. The lowest flow value of asphalt mixtures was 3.01 mm, approximately 20% lower than the control sample's flow value.

The trend of Marshall stability and flow values depicted in Figure 6 is compatible with previous investigations on the effect of CLS on bitumen's stiffness potential [72, 73]. Figure 6(c) shows that when CLS content increased by more than 15% within the bitumen, the brittleness potential of asphalt mixtures soared. Then, the Marshall stability value decreased, and the flow value enlarged. The Marshall test results achieved are in accordance with our earlier observation, which showed that the combination of CLS and bitumen improved the consistency and stiffness of CLS-modified bitumen, leading to improvement in the asphalt mixture's Marshall parameters [33, 39].

Figure 6(c) reveals that the addition of CLS into the bitumen improved the performance of asphalt mixtures against rutting. The MQ values of CLS-modified asphalt mixtures were higher than those of the specimen fabricated by virgin bitumen. As depicted in Figure 6, the MQ values experienced a 64% increase when the CLS content increased from 0% to 15% and hit a peak containing a value of 2.42 kN/mm. Then, asphalt mixtures containing 15% CLS showed the highest resistance to shear stress. The achieved Marshall quotient values were compatible with the findings of McCreedy and Williams [74]. They showed that lignin's presence in asphalt mixtures enhanced the asphalt mixture's rigidity.

*4.2. Resilient Modulus.* Figure 7 shows the resilient modulus values of asphalt mixtures. The resilient modulus test evaluated the response of asphalt mixtures under repeated loadings [75]. Moreover, that test was conducted at 25°C to simulate intermediate temperature conditions for asphalt mixtures [42]. As illustrated in Figure 7, the addition of CLS to the bitumen increased the resilient modulus of asphalt mixtures. The highest resilient modulus was about 17% higher than the resilient modulus of the control sample. More than 15% of CLS into the bitumen brought about a downward trend in resilient modulus values. Therefore, the stiffness of asphalt mixtures improved by adding CLS to the bitumen, which enhanced the asphalt mixture's durability against permanent deformations. On the other hand, an excessive increase in the resilient modulus values reduced the asphalt mixture's flexibility, which was responsible for

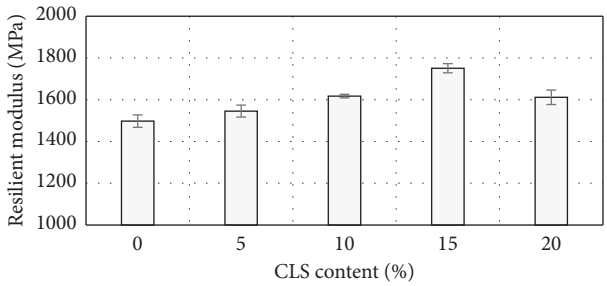


Figure 7: Resilient modulus of asphalt mixtures.

the asphalt mixture's brittleness potential. In accordance with the resilient modulus results of the current study, Prez and others. [76] found that lignin could enhance the stiffness of asphalt mixtures, which led to a 10.48% increase in resilient modulus of asphalt mixtures containing 20% lignin compared with that of the control sample.

Based on the AASHTO flexible pavement design guide and Van Til and others' estimation method, the calculated thickness reduction for surface layers constructed by CLS-modified bitumen is presented in Table 9. It can be concluded that bitumen modification with CLS led to the surface layer's thickness reduction. As shown in Table 9, the thickness of the asphalt mixture containing 15% CLS was 11.61% lower than the thickness of the control sample during the road pavement's construction.

*4.3. Dynamic Creep.* The dynamic creep test was conducted on unmodified and CLS-modified specimens to determine their creep behavior. It is worth mentioning that the dynamic creep test continued until samples reached the third phase of the cumulative strain curve. Three samples were fabricated with the same design procedure for each CLS content and tested using the UTM-14 machine under the same condition. Figure 8 shows that the asphalt mixture with 15% CLS had the lowest cumulative strain values. Moreover, all CLS-modified samples experienced higher rutting resistance than the control sample. The flow number (FN), determined at the end of the second phase of the dynamic creep curve, is reported in Figure 9. As shown in Figure 9, the presence of CLS can delay the plastic failure of the asphalt mixture due to traffic loads. For example, the FN value of the asphalt samples containing 15% CLS was recorded as 1013, which was about 1.8 times higher than the FN value of control samples. These findings are consistent with that of Xu et al. [23], who showed that incorporating lignin into bitumen could enhance the rutting performance of asphalt mixtures at high-temperature levels. Moreover, it is encouraging to compare the dynamic creep test results of the current study with the findings of Zhang et al. [24], who demonstrated that adding 2%, 4%, 6%, and 8% lignin into bitumen improved the resistance of asphalt mixtures against rutting.

*4.4. Wheel Tracking.* Figure 10 demonstrates the curves of rut depth versus passing time derived from the HWT test. It can be observed that in contrast with the rut depth of CLS-modified samples, rut depth was more considerable for control specimens at 60°C. Moreover, the mixture containing 15% CLS had the lowest rut depth, and the control sample had the highest value after 120 minutes. At the end of the HWT experiment, when the CLS content increased from 0% to 15%, a decrease of about 45% in the rut depth was observed. Therefore, CLS had a beneficial impact on the rutting resistance of asphalt mixtures. The HWT test results are compatible with previous research performed by Xie et al. [77], who found that lignin could strengthen the high-temperature performance of asphalt mixtures.

Table 9: Thickness reduction results based on resilient modulus values.

| Mix type | Layer coefficient | Thickness reduction (%) |
|---|---|---|
| CLS-0% | 0.311 | 0 |
| CLS-5% | 0.320 | 2.9 |
| CLS-10% | 0.334 | 7.4 |
| CLS-15% | 0.347 | 11.61 |
| CLS-20% | 0.338 | 8.6 |

Table 10 presents the final rut depth, dynamic stability, and wheel-tracking slope values of the HWT test. It can be found that the rutting parameters (i.e., RD, WTS, and DS) had lower values for CLS-modified samples than for the control specimen. Meanwhile, the samples containing 15% CLS exhibited the highest performance during the HWT test. Then, modification of bitumen by the CLS could effectively improve the rutting performance of asphalt mixtures.

*4.5. Zhou Model and Tukey Method.* Table 11 presents the cycle's repetition number and permanent deformation at transition points of asphalt mixtures based on Zhou's three-stage model. According to Table 11, when the CLS content increased from 0% to 15%, the loading repetition number of primary and secondary stages increased. It can be observed that the stiffness of CLS-modified samples improved their rutting performance. Although 20% CLS decreased the rutting performance of asphalt mixtures compared to those containing 15% CLS, control samples had the highest susceptibility to rutting.

Table 12 explains the findings of the one-way ANOVA conducted by Minitab software. The statistical analysis was performed based on the null hypothesis in which all means were assumed equal. The $p$ value was less than 0.05, indicating that the null hypothesis was unacceptable at the transition points. Then, the $p$ value indicates that the presence of CLS had a significant influence on the rutting performance of asphalt mixtures.

As shown in Table 13, the Tukey method is used to rank the performance of asphalt mixtures in terms of creep behavior. It can be concluded that while the asphalt mixtures containing 15% CLS had the highest rutting performance, control specimens had the lowest rutting performance against traffic loadings. As can be seen from Table 13, the Tukey method did not show any significant differences in second transition point values between samples containing 10% CLS and 20% CLS.

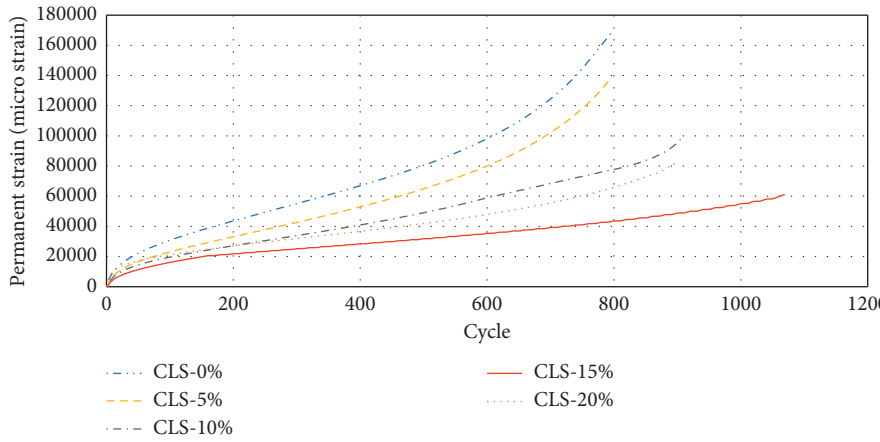


Figure 8: Creep curve for asphalt mixtures.

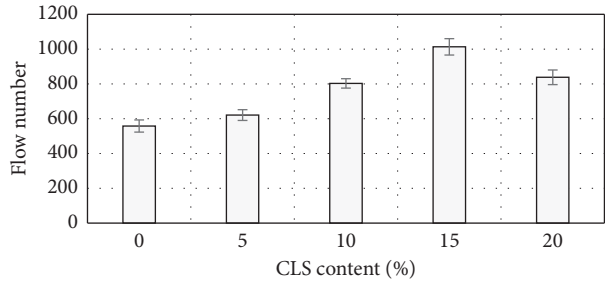


Figure 9: Flow number of asphalt mixtures.

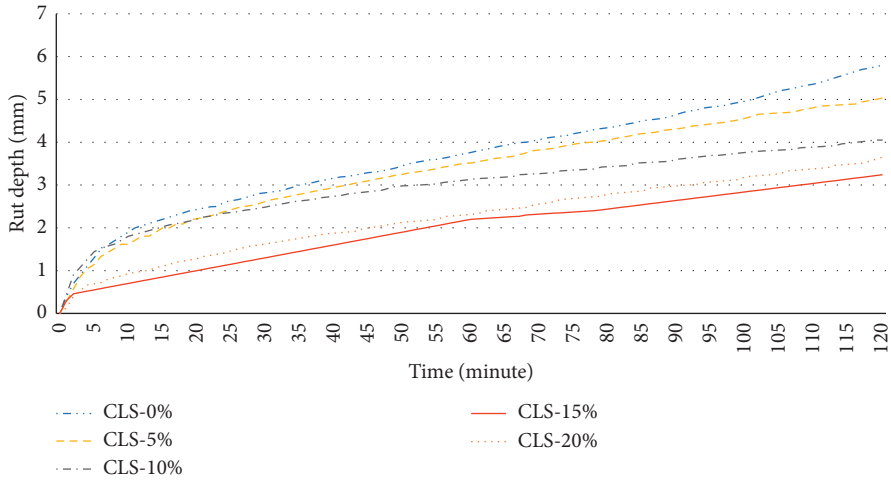


Figure 10: Measurements of the rut depth at 60°C.

Table 10: Final rut depth, wheel-tracking slope, and dynamic stability values of mixtures emanated from the wheel-tracking test.

| Mix type | $RD_{air}$ (mm) | $WTS_{air}$ (mm per $10^3$ cycles) | DS (cycle/min) |
|---|---|---|---|
| CLS-0% | 5.81 | 0.64 | 1554 |
| CLS-5% | 5.04 | 0.48 | 2094 |
| CLS-10% | 4.05 | 0.34 | 2928 |
| CLS-15% | 3.24 | 0.31 | 3351 |
| CLS-20% | 3.65 | 0.41 | 2492 |

Table 11: Creep curve models derived from Zhou's transition points.

| Sample code | First transition point | | Second transition point | |
|---|---|---|---|---|
| | First stage model | End of the first stage | Second stage model | End of the second stage |
| CLS-0% | $\varepsilon_P = 3043.7691N^{0.5044}$ | 107 | $\varepsilon_P = 32142.0423 + 121.9299(N-107)$ | 558 |
| CLS-5% | $\varepsilon_P = 1466.2776N^{0.5279}$ | 135 | $\varepsilon_P = 19536.2273 + 103.2894(N-135)$ | 621 |
| CLS-10% | $\varepsilon_P = 2330.5186N^{0.4641}$ | 146 | $\varepsilon_P = 23546.6286 + 78.4503(N-146)$ | 803 |
| CLS-15% | $\varepsilon_P = 1400.5292N^{0.5302}$ | 160 | $\varepsilon_P = 20655.0756 + 36.3122(N-160)$ | 1013 |
| CLS-20% | $\varepsilon_P = 4630.2121N^{0.3316}$ | 151 | $\varepsilon_P = 24442.7261 + 56.5546(N-151)$ | 828 |

Table 12: One-way ANOVA: transition point values versus CLS content.

| Source | Df | Adj SS | Adj MS | F-value | $P$ value |
|---|---|---|---|---|---|
| First transition point | | | | | |
| CLS content | 4 | 5012.4 | 1253.1 | 55.94 | <0.001 |
| Error | 10 | 224 | 22.4 | | |
| Total | 14 | 5236.4 | | | |
| Second transition point | | | | | |
| CLS content | 4 | 391504 | 97875.9 | 352.83 | <0.001 |
| Error | 10 | 2774 | 277.4 | | |
| Total | 14 | 394278 | | | |

Table 13: Classification of transition points using the Tukey procedure with a confidence level of 95%.

| CLS content (%) | N | Mean | Grouping | | | |
|---|---|---|---|---|---|---|
| First transition point | | | | | | |
| 15 | 3 | 160 | A | | | |
| 20 | 3 | 151 | A | B | | |
| 10 | 3 | 146 | | B | C | |
| 5 | 3 | 135 | | | C | |
| 0 | 3 | 107 | | | | D |
| Second transition point | | | | | | |
| 15 | 3 | 1013 | A | | | |
| 20 | 3 | 828 | | B | | |
| 10 | 3 | 803 | | B | | |
| 5 | 3 | 621 | | | C | |
| 0 | 3 | 558 | | | | D |

## 5. Conclusions

The following results can be obtained with regard to the effects of adding CLS as a bitumen modifier in hot mix asphalt mixtures:

(i) The bumpy surface structure of CLS particles was detected through the FESEM test. Moreover, metal oxides, carbon, magnesium, calcium, and silicon were the significant elements of CLS, according to the EDX analysis.

(ii) Although the Marshall stability of CLS-modified asphalt mixtures recorded higher values than control samples, the flow outputs of asphalt mixtures containing the CLS powder had lower values than the control specimen. As a result, the presence of CLS increased the stiffness of asphalt mixtures. According to the Marshall quotient values, the highest stiffness was achieved for the asphalt mixture containing 15% CLS.

(iii) The incorporation of CLS into bitumen improved the response of the asphalt mixture to cyclic loadings because CLS-modified asphalt mixtures had a higher resilient modulus than control specimens. Moreover, CLS could decrease the thickness of the surface layer, leading to cost-benefit features during the road construction process.

(iv) The addition of CLS into bitumen enhanced the rutting performance of asphalt mixtures against cyclic loadings. Among the four kinds of asphalt mixtures made by 5%, 10%, 15%, and 20% CLS, the asphalt mixture with 15% CLS demonstrated the highest resistance to cyclic loadings during the dynamic creep test.

(v) Increasing the CLS content up to 15% achieved the lowest value of rut depth during the wheel-tracking test. The rutting susceptibility of asphalt mixtures experienced an upward trend when the CLS content increased more than 15%.

(vi) In future investigations, it will be interesting to evaluate the rutting performance of asphalt mixtures containing CLS powder based on different loading shapes during the dynamic creep test. Moreover, further research can investigate the temperature and loading's frequency interactive

effects on the rutting potential of CLS-modified asphalt mixtures based on the response surface methodology.

## Data Availability

Based on the logical request of the responsible author, all data supporting the conclusion of this research will be available.

## Conflicts of Interest

The authors state that there are no conflicts of interest associated with the publication of this study.

## References


[1] X. Yang, A. Shen, Y. Jiang, Y. Meng, and H. Wu, "Properties and mechanism of flame retardance and smoke suppression in asphalt binder containing organic montmorillonite," *Construction and Building Materials*, vol. 302, Article ID 124148, 2021.

[2] Z. Zhang, A. Sha, X. Liu et al., "State-of-the-art of porous asphalt pavement: experience and considerations of mixture design," *Construction and Building Materials*, vol. 262, Article ID 119998, 2020.

[3] G. H. Hamedi, M. R. Esmaeeli, V. Najafi Moghaddam Gilani, and S. M. Hosseinian, "The effect of aggregate-forming minerals on thermodynamic parameters using surface free energy concept and its relationship with the moisture susceptibility of asphalt mixtures," *Advances in Civil Engineering*, vol. 2021, 2021.

[4] X. Wang and Y. Zhong, "Reflective crack in semi-rigid base asphalt pavement under temperature-traffic coupled dynamics using XFEM," *Construction and Building Materials*, vol. 214, pp. 280–289, 2019.

[5] M. Zheng, Y. Tian, and L. He, "Analysis on environmental thermal effect of functionally graded nanocomposite heat reflective coatings for asphalt pavement," *Coatings*, vol. 9, no. 3, p. 178, 2019.

[6] M. Irfan, Y. Ali, S. Ahmed, S. Iqbal, and H. Wang, "Rutting and fatigue properties of cellulose fiber-added stone mastic asphalt concrete mixtures," *Advances in Materials Science and Engineering*, vol. 2019, Article ID 5604197, 8 pages, 2019.

[7] T. Ahmed, E. Y. Hajj, A. Warrag, and M. Piratheepan, "Postmortem evaluation of accelerated rate of raveling of in-service asphalt pavements in arid climatic conditions-case of Kuwait," *Case Studies in Construction Materials*, vol. 14, Article ID e00533, 2021.

[8] H.-P. Wang, Y.-X. Guo, M.-Y. Wu, K. Xiang, and S.-R. Sun, "Review on structural damage rehabilitation and performance assessment of asphalt pavements," *Reviews on Advanced Materials Science*, vol. 60, no. 1, pp. 438–449, 2021.

[9] J. Zhang, H. Li, P. Liu et al., "Experimental exploration of influence of recycled polymer components on rutting resistance and fatigue behavior of asphalt mixtures," *Journal of Materials in Civil Engineering*, vol. 32, no. 6, Article ID 04020129, 2020.

[10] Y. Xu and L. Sun, "Study on permanent deformation of asphalt mixtures by single penetration repeated shear test," *Procedia - Social and Behavioral Sciences*, vol. 96, pp. 886–893, 2013.

[11] H. Majidifard, B. Jahangiri, P. Rath, L. Urra Contreras, W. G. Buttlar, and A. H. Alavi, "Developing a prediction model for rutting depth of asphalt mixtures using gene expression programming," *Construction and Building Materials*, vol. 267, Article ID 120543, 2021.

[12] W. Rafiq, M. A. Musarat, M. Altaf et al., "Life cycle cost analysis comparison of hot mix asphalt and reclaimed asphalt pavement: a case study," *Sustainable Times*, vol. 13, 2021.

[13] S. Kocak and M. Emin Kutay, "Combined effect of SBS and devulcanized rubber (DVR) modification on performance grade and fatigue cracking resistance of asphalt binders," *RILEM Bookseries*, vol. 13, pp. 269–274, 2016.

[14] H. Singh, T. Chopra, S. Jain, A. Kaur, and S. Kamotra, "Effect of aggregate type and polymer modification on the performance of bituminous concrete mixes," *Int. J. Appl. Sci. Eng.*vol. 16, pp. 1–13, 2019.

[15] J. V. S. de Melo, G. Trichês, and L. T. de Rosso, "Experimental evaluation of the influence of reinforcement with Multi-Walled Carbon Nanotubes (MWCNTs) on the properties and fatigue life of hot mix asphalt," *Construction and Building Materials*, vol. 162, pp. 369–382, 2018.

[16] P. J. Yoo and T. W. Kim, "Strengthening of hot-mix asphalt mixtures reinforced by polypropylene-impregnated multifilament glass fibres and scraps," *Construction and Building Materials*, vol. 75, pp. 415–420, 2015.

[17] S. A. Ghanoon, J. Tanzadeh, and M. Mirsepahi, "Laboratory evaluation of the composition of nano-clay, nano-lime and SBS modifiers on rutting resistance of asphalt binder," *Construction and Building Materials*, vol. 238, Article ID 117592, 2020.

[18] J. Yu, M. Vaidya, G. Su, S. Adhikari, E. Korolev, and S. Shekhovtsova, "Experimental study of soda lignin powder as an asphalt modifier for a sustainable pavement material," *Construction and Building Materials*, vol. 298, Article ID 123884, 2021.

[19] S. Ren, X. Liu, Y. Zhang et al., "Multi-scale characterization of lignin modified bitumen using experimental and molecular dynamics simulation methods," *Construction and Building Materials*, vol. 287, Article ID 123058, 2021.

[20] A. Grossman and W. Vermerris, "Lignin-based polymers and nanomaterials," *Current Opinion in Biotechnology*, vol. 56, pp. 112–120, 2019.

[21] J. Wu, Q. Liu, C. Wang, W. Wu, and W. Han, "Investigation of lignin as an alternative extender of bitumen for asphalt pavements," *Journal of Cleaner Production*, vol. 283, Article ID 124663, 2021.

[22] K. B. Batista, R. P. L. Padilha, T. O. Castro et al., "High-temperature, low-temperature and weathering aging performance of lignin modified asphalt binders," *Industrial Crops and Products*, vol. 111, pp. 107–116, 2018.

[23] G. Xu, H. Wang, and H. Zhu, "Rheological properties and anti-aging performance of asphalt binder modified with wood lignin," *Construction and Building Materials*, vol. 151, pp. 801–808, 2017.

[24] Y. Zhang, X. Wang, G. Ji et al., "Mechanical performance characterization of lignin-modified asphalt mixture," *Applied Sciences*, vol. 10, no. 9, p. 3324, 2020.

[25] B. Javilla, H. Fang, L. Mo, B. Shu, and S. Wu, "Test evaluation of rutting performance indicators of asphalt mixtures," *Construction and Building Materials*, vol. 155, pp. 1215–1223, 2017.

[26] M. Irfan, Y. Ali, S. Iqbal, S. Ahmed, and I. Hafeez, "Rutting evaluation of asphalt mixtures using static, dynamic, and repeated creep load tests," *Arabian Journal for Science and Engineering*, vol. 43, no. 10, pp. 5143–5155, 2017.

[27] A. Khodaii and A. Mehrara, "Evaluation of permanent deformation of unmodified and SBS modified asphalt mixtures using dynamic creep test," *Construction and Building Materials*, vol. 23, no. 7, pp. 2586–2592, 2009.

[28] H. Ziari, M. Nakhaei, A. Akbari Nasrekani, and A. Moniri, "Characterization of rutting resistance of EBS-modified asphalt mixtures," *Petroleum Science and Technology*, vol. 34, no. 13, pp. 1107–1112, 2016.

[29] L. N. Mohammad, M. Elseifi, W. Cao, A. Raghavendra, and M. Ye, "Evaluation of various hamburg wheel-Tracking devices and AASHTO T 324 specification for rutting testing of asphalt mixtures," *Asph. Paving Technol. Assoc. Asph. Paving Technol. Tech. Sess.*vol. 86, pp. 165–185, 2017.

[30] H. Y. Katman, M. R. Ibrahim, M. R. Karim, N. Salim Mashaan, and S. Koting, "Evaluation of permanent deformation of unmodified and rubber-reinforced SMA asphalt mixtures using dynamic creep test," *Advances in Materials Science and Engineering*, vol. 2015, 2015.

[31] F. Zhou, T. Scullion, and L. Sun, "Verification and modeling of three-stage permanent deformation behavior of asphalt mixes," *Journal of Transportation Engineering*, vol. 130, no. 4, pp. 486–494, 2004.

[32] T. Baghaee Moghaddam, M. Soltani, and M. R. Karim, "Evaluation of permanent deformation characteristics of unmodified and Polyethylene Terephthalate modified asphalt mixtures using dynamic creep test," *Materials & Design*, vol. 53, pp. 317–324, 2014.

[33] S. Fatemi, J. Bolouri Bazaz, and S. A. Ziaee, "Evaluation of rutting and fatigue behaviors of asphalt binders modified with calcium lignosulfonate," *Advances in Civil Engineering*, vol. 2021, 2021.

[34] R. El Hage, N. Brosse, L. Chrusciel, C. Sanchez, P. Sannigrahi, and A. Ragauskas, "Characterization of milled wood lignin and ethanol organosolv lignin from miscanthus," *Polymer Degradation and Stability*, vol. 94, no. 10, pp. 1632–1638, 2009.

[35] J. Hu, Q. Zhang, and D.-J. Lee, "Kraft lignin biorefinery: a perspective," *Bioresource Technology*, vol. 247, pp. 1181–1183, 2018.

[36] P. J. Van Soest, J. B. Robertson, M. B. Hall, and M. C. Barry, "Klason lignin is a nutritionally heterogeneous fraction unsuitable for the prediction of forage neutral-detergent fibre digestibility in ruminants," *British Journal of Nutrition*, vol. 124, no. 7, pp. 693–700, 2020.

[37] X. Lu, X. Zhu, H. Guo et al., "Investigation on the thermal degradation behavior of enzymatic hydrolysis lignin with or without steam explosion treatment characterized by TG-FTIR and Py-GC/MS," *Biomass Convers. Biorefinery*, vol. 342, pp. 1–10, 2020.

[38] T. Aro and P. Fatehi, "Production and application of lignosulfonates and sulfonated lignin," *ChemSusChem*, vol. 10, no. 9, pp. 1861–1877, 2017.

[39] S. Fatemi, J. B. Bazaz, and S. A. Ziaee, "The pros and cons of using calcium lignosulfonate as a recycled anti-aging additive on engineering properties of bituminous mastics," *Case Studies in Construction Materials*, vol. 15, Article ID e00739, 2021.

[40] C. Xu and F. Ferdosian, "Structure and properties of lignin," *Conversion of Lignin into Bio-Based Chemicals and Materials. Green Chemistry and Sustainable Technology*, Springer, Berlin, Heidelberg, pp. 1–12, 2017.

[41] K. S. Khitrin, S. L. Fuks, S. V. Khitrin, S. A. Kazienkov, and D. S. Meteleva, "Lignin utilization options and methods," *Russian Journal of General Chemistry*, vol. 82, no. 5, pp. 977–984, 2012.

[42] S. Fatemi and R. Imaninasab, "Performance evaluation of recycled asphalt mixtures by construction and demolition waste materials," *Construction and Building Materials*, vol. 120, pp. 450–456, 2016.

[43] A. Gobetti, G. Cornacchia, and G. Ramorino, "Innovative reuse of electric arc furnace slag as filler for different polymer matrixes," *Minerals*, vol. 11, no. 8, p. 832, 2021.

[44] H. Ziari, M. Naghavi, and R. Imaninasab, "Performance evaluation of rubberised asphalt mixes containing WMA additives," *International Journal of Pavement Engineering*, vol. 19, no. 7, pp. 623–629, 2018.

[45] S. Aflaki and N. Tabatabaee, "Proposals for modification of Iranian bitumen to meet the climatic requirements of Iran," *Construction and Building Materials*, vol. 23, no. 6, pp. 2141–2150, 2009.

[46] X. Ouyang, X. Qiu, and P. Chen, "Physicochemical characterization of calcium lignosulfonate-A potentially useful water reducer," *Colloids Surfaces A Physicochem. Eng. Asp.*vol. 282–283, pp. 489–497, 2006.

[47] K. K. Khichar, S. B. Dangi, V. Dhayal et al., "Structural, optical, and surface morphological studies of ethyl cellulose/graphene oxide nanocomposites," *Polymer Composites*, vol. 41, no. 7, pp. 2792–2802, 2020.

[48] J. O. Akinyele, R. W. Salim, and W. K. Kupolati, "The impact of rubber crumb on the mechanical and chemical properties of concrete," *Engineering Structures and Technologies*, vol. 7, no. 4, pp. 197–204, 2016.

[49] Y. Zhang, X. Liu, P. Apostolidis et al., "Chemical and rheological evaluation of aged lignin-modified bitumen," *Materials*, vol. 12, no. 24, p. 4176, 2019.

[50] P. Jędrzejczak, M. N. Collins, T. Jesionowski, and Ł. Klapiszewski, "The role of lignin and lignin-based materials in sustainable construction – a comprehensive review," *International Journal of Biological Macromolecules*, vol. 187, pp. 624–650, 2021.

[51] M. A. Kadhim, S. Al-Busaltan, and R. R. Almuhanna, "An evaluation of the effect of crushed waste glass on the performance of cold bituminous emulsion mixtures," *International Journal of Pavement Research and Technology*, vol. 12, no. 4, pp. 396–406, 2019.

[52] A. I. Al-Hadidy, "Performance of SBS-hma mixes made with sasobit and zeolite," *Journal of Materials in Civil Engineering*, vol. 32, no. 10, Article ID 06020017, 2020.

[53] N. M. Asmael and M. Q. Waheed, "Investigation of using polymers to improve asphalt pavement performance," *Am. Sci. Res. J. Eng. Technol. Sci.*vol. 39, pp. 38–48, 2018, http://asrjetsjournal.org/index.php/American_Scientific_Journal/article/download/3768/1364 accessed.

[54] H. Chen, Q. Xu, S. Chen, and Z. Zhang, "Evaluation and design of fiber-reinforced asphalt mixtures," *Materials & Design*, vol. 30, no. 7, pp. 2595–2603, 2009.

[55] R. Mistry and T. Kumar Roy, "Predicting Marshall stability and flow of bituminous mix containing waste fillers by fuzzy logic," *Revista de la construcción*, vol. 19, no. 2, pp. 209–219, 2020.

[56] M. Ameri, S. Hesami, and H. Goli, "Laboratory evaluation of warm mix asphalt mixtures containing electric arc furnace (EAF) steel slag," *Construction and Building Materials*, vol. 49, pp. 611–617, 2013.

[57] H. Ziari, A. Moniri, R. Imaninasab, and M. Nakhaei, "Effect of copper slag on performance of warm mix asphalt," *International Journal of Pavement Engineering*, vol. 20, no. 7, pp. 775–781, 2019.

[58] R. H. Ariyapijati, S. P. Hadiwardoyo, and R. J. Sumabrata, "Contributions crumb rubber in hot mix asphalt to the

resilient modulus," *AIP Conference Proceedings*, vol. 1855, Article ID 030005, 2017.

[59] M. K. Idham, H. Mohd Rosli, H. Yaacob, M. N. M. Warid, and M. E. Abdullah, "Effect of aging on resilient modulus of hot mix asphalt mixtures," *Advanced Materials Research*, vol. 723, pp. 291–297, 2013.

[60] G. Shafabakhsh and A. Tanakizadeh, "Investigation of loading features effects on resilient modulus of asphalt mixtures using Adaptive Neuro-Fuzzy Inference System," *Construction and Building Materials*, vol. 76, pp. 256–263, 2015.

[61] A. Azarhoosh, M. Koohmishi, and G. H. Hamedi, "Rutting resistance of hot mix asphalt containing coarse recycled concrete aggregates coated with waste plastic bottles," *Advances in Civil Engineering*, vol. 2021, pp. 1–11, Article ID 9558241, 2021.

[62] N. Li, H. Zhan, X. Yu, W. Tang, H. Yu, and F. Dong, "Research on the high temperature performance of asphalt pavement based on field cores with different rutting development levels," *Mater. Struct. Constr.*vol. 54, 2021.

[63] E. Y. Hajj, A. Ulloa, R. Siddharthan, and P. E. Sebaaly, "Characteristics of the loading pulse for the flow number performance test," *Asph. Paving Technol. Assoc. Asph. Paving Technol. Tech. Sess.*vol. 79, pp. 253–285, 2010, https://trid.trb.org/view/1087096 accessed.

[64] T. A. Sangita, S. Khan, D. K. Sabina, and D. K. Sharma, "Effect of waste polymer modifier on the properties of bituminous concrete mixes," *Construction and Building Materials*, vol. 25, no. 10, pp. 3841–3848, 2011.

[65] P. Zieliński, "Indirect tensile test as a simple method for rut resistance evaluation of asphalt mixtures–Polish experience," *Road Materials and Pavement Design*, vol. 23, no. 1, pp. 112–128, 2020.

[66] Y. Zhao, Y. Gao, K. Zhang, Y. Zhang, and M. Yu, "Establishment of rutting model of wheel-tracking test for real-time prediction of rut depth of asphalt layers," *Advances in Civil Engineering*, vol. 2021, pp. 1–16, 2021.

[67] P. Chaturabong and H. U. Bahia, "Mechanisms of asphalt mixture rutting in the dry Hamburg Wheel Tracking test and the potential to be alternative test in measuring rutting resistance," *Construction and Building Materials*, vol. 146, pp. 175–182, 2017.

[68] D. Movilla-Quesada, A. C. Raposeiras, L. T. Silva-Klein, P. Lastra-González, and D. Castro-Fresno, "Use of plastic scrap in asphalt mixtures added by dry method as a partial substitute for bitumen," *Waste Management*, vol. 87, pp. 751–760, 2019.

[69] Q. Lv, W. Huang, M. Zheng, H. Sadek, Y. Zhang, and C. Yan, "Influence of gradation on asphalt mix rutting resistance measured by Hamburg Wheel Tracking test," *Construction and Building Materials*, vol. 238, p. 117674, 2020.

[70] X. Yan, R. Ying, J. Jin, and Y. Zhang, "Study on cracking resistance of basalt fiber-reinforced microbond asphalt macadam," *Advances in Civil Engineering*, vol. 2021, 2021.

[71] H. Ziari, A. T. Barakoohi, and A. Moniri, "Laboratory investigation of the effect of temperature on frictional properties of concrete pavements containing crushed glass," *International Journal of Pavement Research and Technology*, vol. 10, no. 4, pp. 297–303, 2017.

[72] M. Zarei, A. Abdi Kordani, and M. Zahedi, "Pure mode I and pure mode II fracture resistance of modified hot mix asphalt at low and intermediate temperatures," *Fatigue and Fracture of Engineering Materials and Structures*, vol. 44, no. 8, pp. 2222–2243, 2021.

[73] M. Zarei, A. Abdi Kordani, Z. ghamarimajd, M. khajehzadeh, M. Khanjari, and M. Zahedi, "Evaluation of fracture resistance of asphalt concrete involving Calcium Lignosulfonate and Polyester fiber under freeze-thaw damage," *Theoretical and Applied Fracture Mechanics*, vol. 117, Article ID 103168, 2022.

[74] N. S. McCready and R. C. Williams, "Utilization of biofuel coproducts as performance enhancers in asphalt binder," *Transportation Research Record: Journal of the Transportation Research Board*, vol. 2051, no. 1, pp. 8–14, 2008.

[75] M. Karami, H. Nikraz, S. Sebayang, and L. Irianti, "Laboratory experiment on resilient modulus of BRA modified asphalt mixtures," *International Journal of Pavement Research and Technology*, vol. 11, no. 1, pp. 38–46, 2018.

[76] I. P. Pérez, A. M. Rodríguez Pasandín, J. C. Pais, and P. A. Alves Pereira, "Use of lignin biopolymer from industrial waste as bitumen extender for asphalt mixtures," *Journal of Cleaner Production*, vol. 220, pp. 87–98, 2019.

[77] S. Xie, Q. Li, P. Karki, F. Zhou, and J. S. Yuan, "Lignin as renewable and superior asphalt binder modifier," *ACS Sustainable Chemistry & Engineering*, vol. 5, no. 4, pp. 2817–2823, 2017.